

UDK 524.77

OPTICAL IDENTIFICATION OF ACTIVE GALACTIC NUCLEUS CANDIDATES DETECTED BY THE MIKHAIL PAVLINSKY ART-XC TELESCOPE ABOARD THE SRG OBSERVATORY DURING THE ALL-SKY X-RAY SURVEY

© 2022 I.A. Zaznabin^{1*}, G.S. Uskov¹, S.Yu. Sazonov¹, R.A. Burenin¹, P.S. Medvedev¹,
G.A. Khorunzhev¹, A.R. Lyapin¹, R.A. Krivonos¹, E.V. Filippova¹, M.R. Gilfanov^{1,2},
R.A. Sunyaev^{1,2}, M.V. Eselevich³, I.F. Bikmaev^{4,5}, E.N. Irtuganov⁴, E.A. Nikolaeva⁴

¹Space Research Institute, Profsoyuznaya str. 84/32, Moscow, 117997 Russia

²Max Planck Institut für Astrophysik, Karl-Schwarzschild-Str. 1, Postfach 1317, D-85741 Garching, Germany

³Institute of Solar–Terrestrial Physics, Russian Academy of Sciences, Siberian Branch, P.O. Box 291, Irkutsk, 664033 Russia

⁴Kazan Federal University, Kremlevskaya str. 18, Kazan, 420000 Russia

⁵Academy of Sciences of Tatarstan, Baumana str. 20, Kazan, Russia

Submitted November 26, 2020

We present the results of our identification of eight objects from a preliminary catalogue of X-ray sources detected in the 4–12 keV energy band by the Mikhail Pavlinsky ART-XC telescope aboard the SRG observatory during its first all-sky survey. Three of them (SRGA J005751.0 + 210846, SRGA J014157.0 – 032915, SRGA J232446.8 + 440756) have been discovered by ART-XC, while five were already known previously as X-ray sources, but their nature remained unknown. The last five sources have also been detected in soft X-rays by the eROSITA telescope of the SRG observatory. Our optical observations were carried out at the 1.6-m AZT-33IK telescope of the Sayan Observatory and the 1.5-m Russian–Turkish telescope (RTT-150). All of the investigated objects have turned out to be active galactic nuclei (AGNs) at redshifts from 0.019 to 0.283. Six of them are Seyfert 2 galaxies (including one Seyfert 1.9 galaxy), one (SRGA J005751.0+210846) is a “hidden” AGN (in an edge-on galaxy), and one (SRGA J224125.9 + 760343) is a narrow-line Seyfert 1 galaxy. The latter object is characterized by a high X-ray luminosity ($\sim (2 - 13) \times 10^{44} \text{ erg s}^{-1}$ in the 4–12 keV band) and, according to our black hole mass estimate ($\sim 2 \times 10^7 M_\odot$), an accretion rate close to the Eddington limit. All three AGNs discovered by the ART-XC telescope (which are not detected by the eROSITA telescope) are characterized by a high absorption column density ($N_H \gtrsim 3 \times 10^{23} \text{ cm}^{-2}$). The results obtained confirm the expectations that the ART-XC telescope is an efficient instrument for searches of heavily obscured and other interesting AGNs in the nearby ($z \lesssim 0.3$) Universe. The SRG all-sky survey will last for more than 3 years more, which will allow many such objects to be discovered.

Key words: active galactic nuclei, sky surveys, optical observations, redshifts, X-ray observations.

INTRODUCTION

The Russian Mikhail Pavlinsky ART-XC telescope (Pavlinski et al., 2021) aboard the Russian SRG orbital observatory (Sunyaev et al., 2021) has been conducting an all-sky X-ray survey at energies from 4 to 30 keV since December 2019. Mirrors operating on the principle of grazing X-ray incidence and semiconductor detectors based on cadmium telluride crystals are used in the telescope, providing unique characteristics for this energy range: a

wide field of view (36 arcmin) and good angular resolution (better than 1 arcmin in the sky scanning mode). Because of this, during the four-year survey we expect to obtain an all-sky map unique in depth and sharpness at energies 4–12 keV and, in particular, to detect at least 5000 active galactic nuclei (AGNs), which is several times more than has been found at such energies in previous all-sky surveys.

In June 2020, the SRG observatory completed the first (of the planned eight) all-sky scans, and a preliminary catalogue of detected sources (more

* e-mail: zaznabin@iki.rssi.ru

than 600 objects in total) was produced from the ART-XC data obtained. This catalogue was correlated with: (1) catalogues of sources detected in previous X-ray sky surveys; (2) the preliminary catalogue of sources detected on one half of the celestial sphere $0 < |l| < 180^\circ$ ¹ in the soft X-ray energy band during the first SRG/eROSITA survey; (3) catalogues of astrophysical objects in other wavelength ranges (from radio to ultraviolet). As a result, a list of objects consisting of the sources discovered by the ART-XC telescope and previously known X-ray sources of unknown nature was compiled. Some of these objects were also detected by the eROSITA telescope (Predehl et al., 2020) of the SRG observatory.

Spectroscopic observations are carried out at Russian optical telescopes to identify these potentially interesting ART-XC sources. The first results of this observational campaign are presented in the present paper. The eight ART-XC sources to be discussed below have proved to be type 1 or 2 AGNs, including objects with strong internal absorption. The latter was revealed by analyzing the X-ray spectra constructed from the ART-XC and eROSITA data.

The presented luminosity estimates are based on the model of a flat Universe with parameters $H_0 = 70$ and $\Omega_m = 0.3$.

THE SAMPLE OF OBJECTS

The objects being studied (see Table 1) were selected among the point X-ray sources detected by the ART-XC telescope during the first sky survey (December 12, 2019–June 10, 2020) with a signal-to-noise ratio of no less than 4.5 in the 4–12 keV energy band. Based on the ART-XC data, we measured the positions of the sources in the sky and their fluxes in this energy band. The typical position error (at 95% confidence) is 30 arcsec.

For these objects, based on the eROSITA data, we obtained the fluxes or upper limits on the flux in three energy bands: 0.3–2, 2–6, and 4–9 keV. Out of the eight sources detected by the ART-XC telescope, 5 were also detected by the eROSITA telescope either in all three or in the first two of these bands. For them, based on the eROSITA data, we managed to improve the source position in the sky. The remaining three objects are not detected by the eROSITA telescope.

For all our objects Table 1 gives: the coordinates

¹Russian scientists are responsible for processing the data from the eROSITA telescope (Germany) in this part of the sky.

of the ART-XC source, the coordinates of the putative optical counterpart, the distance between the position of the optical counterpart and the positions of the X-ray source from the ART-XC and eROSITA data (if available), and the X-ray observatory that first discovered the X-ray source.

X-RAY OBSERVATIONS

The X-ray radiation from AGNs can experience photoabsorption in the gas–dust torus around the supermassive black hole (SMBH) and in the interstellar medium of the host galaxy. One of the goals of this study was to estimate the column density of neutral (or weakly ionized) matter N_H for the objects being discussed. Although the number of X-ray photons detected by the ART-XC and eROSITA telescopes (in the short source scanning time during the SRG sky survey) is insufficient to perform a detailed spectral analysis, these data nevertheless allow sufficiently reliable constraints on N_H to be obtained in most cases.

We fitted the X-ray spectra in the range 0.3–12 keV using the XSPEC v12.9.0n2² code jointly based on the ART-XC and eROSITA data. The spectra were first binned in such a way that there were at least three counts in each spectral bin.

We assumed the AGN X-ray spectrum to be fitted by a power law with a fixed slope $\Gamma = 1.8$ (a typical value for Seyfert galaxies) and a low-energy cutoff as a result of photoabsorption in the Galaxy and the object itself. Thus, we used the following model in XSPEC:

$$phabs(zphabs(powerlaw)),$$

where *phabs* is the absorption in the Galaxy from HI4PI survey data (Bekhti et al., 2016) and *zphabs* is the absorption at the AGN redshift *z* (measured from the object’s optical spectrum). A satisfactory quality of the fit was achieved for all of the sources.

The X-ray spectra obtained are presented on the graphs below in units of $F_E(E)$. A power-law model with a slope $\Gamma = 1.8$ was used to convert the counts on the detector to photons. It should be kept in mind that such figures should not be used to obtain accurate fluxes.

OPTICAL OBSERVATIONS

Our spectroscopy for the objects was performed at the 1.6-m AZT-33IK telescope of the Sayan Observatory using the low- and medium-resolution

²<https://heasarc.gsfc.nasa.gov/xanadu/xspec/>

ART-XC source	Optical coordinates		r (ART-XC)	r (eROSITA)	Discovered by
	α	δ			
SRGA J005751.0+210846	00 57 52.1	+21 08 46	15.4''	–	SRG
SRGA J014157.0–032915	01 41 59.4	–03 29 34	40.6''	–	SRG
SRGA J043209.6+354917	04 32 08.0	+35 49 29	22.9''	2.3''	ROSAT
SRGA J045049.8+301449	04 50 48.0	+30 15 03	27.2''	3.2''	Swift
SRGA J152102.3+320418	15 21 01.8	+32 04 14	7.5''	2.9''	Swift
SRGA J200431.6+610211	20 04 32.4	+61 02 31	20.8''	5.3''	ROSAT
SRGA J224125.9+760343	22 41 25.8	+76 03 53	10.0''	4.6''	ROSAT
SRGA J232446.8+440756	23 24 48.4	+44 07 57	17.3''	–	SRG

Column 1: the source name in the preliminary ART-XC catalogue (the coordinates of the X-ray sources used in the names are given for epoch J2000.0). Columns 2 and 3: the coordinates of the putative optical counterpart. Column 4: the distance between the ART-XC source position and the optical counterpart position. Column 5: the separation between the eROSITA source position and the optical counterpart position (the dash means that a given source is not detected by the eROSITA telescope). Column 6: the X-ray observatory that discovered the source.

Table 1. List of objects for our spectroscopic observations

ADAM spectrograph (Afanasiev et al., 2016; Burenin et al., 2016) and the 1.5-m Russian–Turkish telescope (RTT-150) using the TFOSC³ spectrograph. A set of long slits is used at both spectrographs to obtain the spectra.

We used volume phase holographic gratings (VPHG), 600 lines per millimeter, to obtain the spectra at the ADAM spectrograph. As a dispersive element we used VPHG600G for the spectral range 3650–7250 Å with a resolution of 4.3 Å and VPHG600R for the spectral range 6460–10 050 Å with a resolution of 6.1 Å. When using VPHG600R, we set the OS11 filter, which removes the second interference order from the image. A thick e2v CCD30-11 array produced by the deep depletion technology is installed at the spectrograph. This allows the spectral images to be obtained at a wavelength of 1 μm without interference on the thin CCD substrate. A set of slits is available at the spectrograph; we used a 2''-wide slit to obtain the spectroscopic images. All our observations were performed with zero slit position angle. After each series of spectroscopic images for each object, we obtained the calibration images of a lamp with a continuum spectrum and the line spectrum of a He–Ne–Ar lamp.

Transmitting diffraction grating no. 15 with the spectral range 3700–8700 Å, which provides a spectral resolution of 12 Å, was used at the TFOSC spectrograph as a dispersive element. This grating allows bright Balmer lines to be obtained in the spectral images for galaxies up to $z = 0.32$.

³<http://hea.iki.rssi.ru/rtt150/en/index.php?page=tfosc>

To obtain the spectroscopic images, we used a 2''-wide slit. The spectrograph slit position angle is 90°. Before and after obtaining the series of spectroscopic images for each object, we obtained the images of a lamp with a continuum spectrum and the line spectrum of a Fe–Ar lamp.

All our observations were carried out at dark moonless time. Before obtaining the spectroscopic images, we tried to place the galactic nucleus at the center of the spectrograph slit as accurately as possible. After each exposure, we changed the object's position along the slit by 10–15'' in a random direction upward or downward using a photoguide. On each night at both telescopes we took the spectra of spectrophotometric standards from the ESO⁴ list for all the sets of diffraction gratings and slits being used. The data reduction was performed using IRAF⁵ software package and our own software.

To estimate the broadening of emission lines, their profiles were fitted by a Gaussian, with the background having been fitted by a polynomial. The line width was defined as $FWHM = \sqrt{FWHM_{\text{mes}}^2 - FWHM_{\text{res}}^2}$, where $FWHM_{\text{mes}}$ is the measured line width and $FWHM_{\text{res}}$ is the spectral broadening of the instrument whose values were given above for each dispersive element being used.

We classified the Seyfert galaxies based on their optical spectra in a standard way (Osterbrock,

⁴<https://www.eso.org/sci/observing/tools/standards/spectra/stanlis.html>

⁵<http://iraf.noao.edu/>

1981; Véron-Cetty et al., 2001)).

RESULTS OF OBSERVATIONS

Below we present the details of our optical and X-ray observations and the results obtained for each object from the sample.

SRGA J005751.0+210846

This X-ray source was discovered in the 4–12 keV band by the ART-XC telescope of the SRG observatory and, at the same time, was not detected in softer X-rays by the eROSITA telescope of the same observatory.

A probable optical counterpart of the X-ray source is the galaxy LEDA 1643776 that falls into the ART-XC position error circle (Fig. 1). The galaxy is oriented edge-on to the observer. Previously, a spectrum has already been obtained for it during the Sloan Digital Sky Survey (release 12, SDSS Collaboration 2015), from which its redshift was measured ($z = 0.04798 \pm 0.00002$). However, this spectrum does not allow the object to be reliably classified as an AGN.

Our optical observations of the object were carried out on October 22, 2020, at the AZT-33IK telescope with VPHG600G. Six spectral images with an exposure time of 300 s each were obtained; the total exposure time was 30 min.

Our spectrum of the galaxy is shown in Fig. 1. Narrow $H\alpha$, $[NII]\lambda 6584$, and sulfur doublet emission lines are seen in it. The $H\beta$, $[OIII]\lambda 4959$, and $[OIII]\lambda 5007$ lines are absent. The 2σ upper boundary of the intensity maximum in these lines is $5.5 \times 10^{-17} \text{ erg s}^{-1} \text{ cm}^{-2} \text{ \AA}^{-1}$. Table 2 presents the characteristics of the two brightest lines. From these two lines we measured the object's redshift, $z = 0.04795 \pm 0.00005$, consistent with the measured SDSS redshift within the error limits.

Because of the absence of the $H\beta$ line and the $[OIII]$ doublet in the spectrum, it is impossible to establish the position of the galaxy LEDA 1643776 on the standard BPT diagram (Baldwin et al. 1981, see Fig. 9) and, consequently, its optical type. Nevertheless, a high X-ray luminosity ($\sim 5 \times 10^{43} \text{ erg s}^{-1}$ in the 4–12 keV band from the ART-XC data) of the object leaves no doubt that this is an AGN. The weakness of the observed lines probably stems from the fact that we observe the galaxy LEDA 1643776 edge-on, so that the optical radiation from the active nucleus (and, in particular, from the narrow-line region) is almost completely absorbed in the interstellar gas of the galaxy.

The non-detection by the eROSITA telescope in combination with the 4–12 keV flux measured by

the ART-XC telescope (Fig. 1) allows a lower limit (at 90% confidence) to be placed on the absorption column density: $N_H > 10^{24} \text{ cm}^{-2}$. Much of this absorption may arise in the interstellar gas of the galaxy and not in the gas–dust torus surrounding the SMBH.

SRGA J014157.0–032915.

This X-ray source was discovered in the 4–12 keV band by the ART-XC telescope of the SRG observatory and, at the same time, was not detected in softer X-rays by the eROSITA telescope.

A probable optical counterpart is the galaxy LEDA 1070544 (Fig. 2). Although its center is at a distance of about $40''$ from the position of the X-ray source (Table 1), such position errors can occur in the case of sources at the ART-XC detection threshold.

Our optical observations were carried out on October 13, 2020, at the AZT-33IK telescope using VPHG600G. Three spectral images with an exposure time of 600 s each were obtained; the total exposure time was 30 min.

The $H\beta$, $[OIII]\lambda 4959$, $[OIII]\lambda 5007$, $H\alpha$, and $[SII]$ doublet emission lines are seen in our spectrum (Fig. 2). The $[NII]\lambda 6584$ line is difficult to separate from the $H\alpha$ line. Table 3 gives the characteristics of the emission lines. They are all narrow. The redshift determined from four lines is $z = 0.01878 \pm 0.00003$.

The absence of broad lines in the spectrum and a fairly high X-ray luminosity ($\sim 3 \times 10^{42} \text{ erg s}^{-1}$ in the 4–12 keV band from the ART-XC data) suggest that this is a Seyfert 2 galaxy. However, according to the measured line flux ratios $\log([OIII]\lambda 5007/H\beta) = 0.49 \pm 0.09$ and $\log([NII]\lambda 6584/H\alpha) < -0.86$, the object lies in the region of star-forming galaxies on the BPT diagram (Fig. 9), though near (within three standard deviations) the region of Seyfert galaxies. Most likely, we are dealing with a galaxy in which, apart from SMBH activity, there is active star formation.

The non-detection by the eROSITA telescope in combination with the 4–12 keV flux measured by the ART-XC telescope (Fig. 1) allows a lower limit to be placed on the absorption column density: $N_H > 3 \times 10^{23} \text{ cm}^{-2}$. However, this limit cannot yet be deemed reliable, because it was obtained only at 68% confidence. To make sure that there is a strong absorption in this object, it is necessary to take an X-ray spectrum with a significantly larger number of photons.

SRGA J005751.0+210846

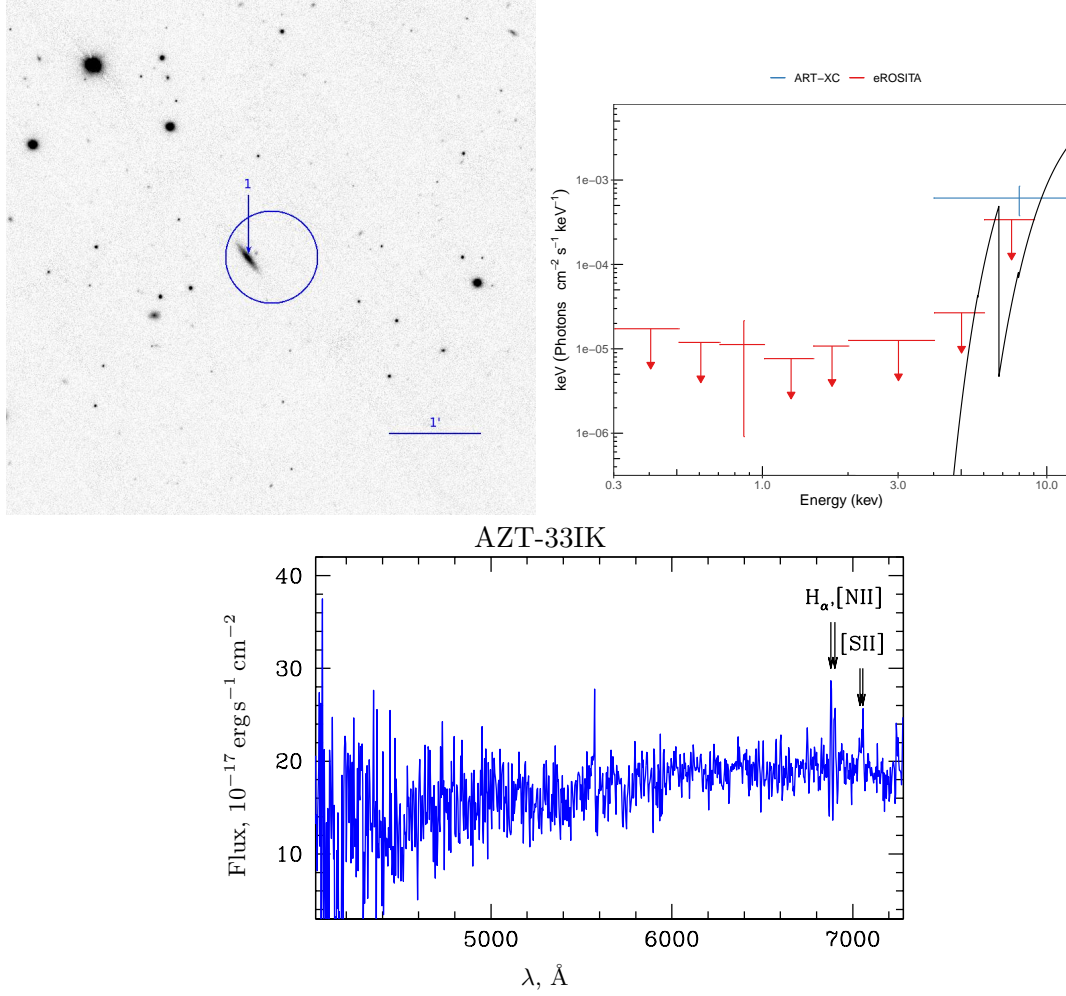


Fig. 1. Top left: the pointing picture for the source SRGA J005751.0+210846 taken from the Pan-STARRS1 survey (Chambers et al., 2016). The arrow indicates the object for which an optical spectrum was taken; the blue circumference marks the ART-XC position error circle of the source 30'' in radius. Top right: the X-ray spectrum from the ART-XC (red) and eROSITA (blue) data and the best-fit model (a power law with absorption) (black line). The arrows indicate the upper limits. Bottom: the optical spectrum with an indication of some emission and absorption lines.

Line	Wavelength, Å	Flux, 10 ⁻¹⁶ erg s ⁻¹ cm ⁻²	Eq. Width ¹ , Å	<i>FWHM</i> , km s ⁻¹
Hα	6880	9.9 ± 6.0	-5.0 ± 3.0	(3.6 ± 0.3) × 10 ²
N II λ6584	6901	8.8 ± 5.0	-4.4 ± 2.5	(3.8 ± 0.2) × 10 ²

¹ Negative values correspond to emission lines.

Table 2. Spectral features of the SRGA J005751.0+210846 = LEDA 1643776

SRGA J014157.0–032915

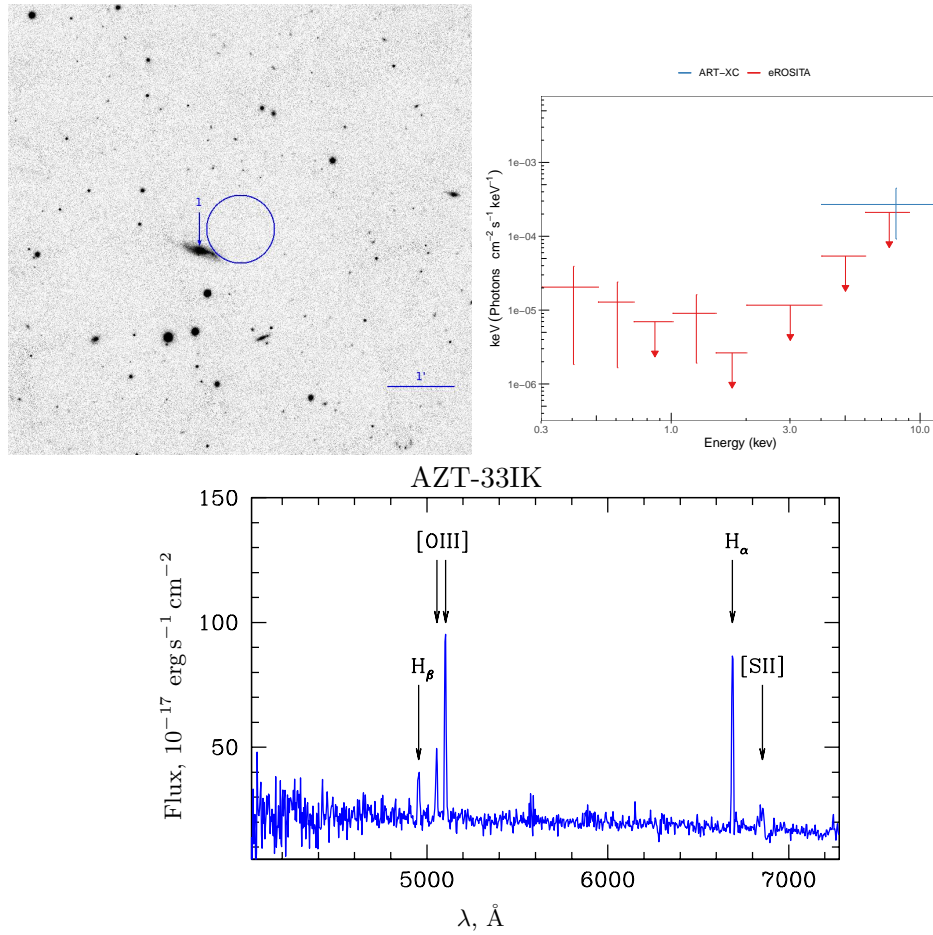


Fig. 2. Same as Fig. 1, but for SRGA J014157.0–032915. No spectral model is shown on the graph with the X-ray spectrum because of the large scatter in model parameters.

Line	Wavelength, Å	Flux, $10^{-16} \text{ erg s}^{-1} \text{ cm}^{-2}$	Eq. Width, Å	$FWHM$, km s^{-1}
H β	4954	27 ± 5	-17.8 ± 3.0	$(6.0 \pm 0.7) \times 10^2$
O III λ 4960	5054	31 ± 3	-14.5 ± 1.5	$(5.0 \pm 0.7) \times 10^2$
O III λ 5007	5102	84 ± 9	-38 ± 4	$(4.9 \pm 0.7) \times 10^2$
H α	6689	88 ± 8	-50 ± 5	$(3.9 \pm 0.5) \times 10^2$
N II λ 6584	6709	< 12	> -7.3	–

Table 3. Spectral features of SRGA J014157.0 – 032915 = LEDA 1070544

SRGA J043209.6+354917

This X-ray source is first mentioned under the name 1WGA J0432.1 + 3549 in the catalogue of sources discovered in the soft X-ray energy band during the ROSAT pointed observations (White et al., 2000). It is also present in the catalogue of sources detected during the XMM-Newton slew observations (The XMM-Newton Survey Science Centre, 2018). However, the nature of this object so far has remained unknown. The source was reliably detected by both ART-XC and eROSITA telescopes of the SRG observatory.

The X-ray source is reliably identified with the galaxy 2MASX J04320796 + 3549287 = WISEA J043207.95 + 354928.8 (Fig. 3), whose colors in the near infrared ($W1 - W2 = 0.68$) (Wright et al., 2010) point to the presence of an active nucleus.

Our optical observations were carried out on September 15, 2020, at RTT-150. Five spectral images with an exposure of 900 s each were obtained; the total exposure time was 75 min.

Balmer hydrogen and forbidden oxygen and nitrogen emission lines are seen in the object's spectrum (Fig. 3). Table 4 gives the characteristics of the emission lines. The redshift was determined from three lines, $H\alpha$, $[\text{O III}]\lambda 5007$, and $[\text{N II}]\lambda 6584$, and is $z = 0.0506 \pm 0.0010$. The $H\alpha$ and $H\beta$ lines have a broad component; only an upper limit can be placed on the flux in the narrow $H\beta$ component. The object is classified from the ratios $\log([\text{O III}]\lambda 5007/H\beta) > 0.77$ and $\log([\text{N II}]\lambda 6584/H\alpha) = 0.19 \pm 0.11$ (Fig. 9) and the fluxes in the broad and narrow $H\alpha$ and $H\beta$ components as a Seyfert 1 galaxy. A slight absorption is detected in the object's X-ray spectrum (Fig. 3): $N_{\text{H}} \sim 3 \times 10^{21} \text{ cm}^{-2}$.

SRGA J045049.8+301449

This object was discovered in hard X-rays (the source SWIFT J0450.6+3015) by the BAT instrument of the Neil Gehrels Swift observatory (Oh et al., 2018) and is present in the catalogue of point X-ray sources detected by the XRT telescope of the same observatory (Evans et al., 2020). However, its nature so far has remained unknown. The source was reliably detected by both ART-XC and eROSITA telescopes of the SRG observatory.

The X-ray source is reliably identified (Fig. 4) with the galaxy LEDA 1896296 = WISEA J045048.00+301502.8 ($W1 - W2 = 0.38$).

Our optical observations were carried out on October 22, 2020, at the AZT-33IK telescope using

VPHG600G. Four spectral images with an exposure time of 600 s each were obtained near the object's culmination; the total exposure time was 40 min.

The $[\text{O III}]\lambda 4960$, $\lambda 5007$, $H\alpha$, $[\text{N II}]\lambda 6584$, and sulfur doublet emission lines are seen in the object's spectrum (Fig. 4). The $H\beta$ line is unseen. The upper limit on the ratio $\log([\text{O III}]\lambda 5007/H\beta) > 0.92$. The upper limit on the ratio $\log([\text{N II}]\lambda 6584/H\alpha) = -0.04 \pm 0.16$. All these lines are narrow, except $H\alpha$ in which a broad component can be distinguished.

The characteristics of the emission lines are given in Table 5. The object's redshift was measured from six emission lines: $z = 0.03308 \pm 0.00004$. From the position on the BPT diagram (Fig. 9) and the presence of a broad component only in the Balmer $H\alpha$ line, the object can be classified as a Seyfert 1.9 galaxy.

An appreciable absorption is detected in the object's X-ray spectrum (Fig. 4): $N_{\text{H}} \sim 4 \times 10^{22} \text{ cm}^{-2}$.

SRGA J152102.3+320418

This X-ray source is present in the catalogue of point X-ray sources detected by the XRT telescope of the Neil Gehrels Swift observatory (Evans et al., 2020), but its nature so far has remained unknown. The source was reliably detected by both ART-XC and eROSITA telescopes of the SRG observatory.

The X-ray source is reliably identified (Fig. 5) with the galaxy (SDSS data) WISEA J152101.83+320414.6, whose infrared color ($W1 - W2 = 1.20$) points to the possible presence of an active nucleus.

Our optical observations were carried out on February 27 and April 24, 2020, at the AZT-33IK telescope. Five spectral images with an exposure time of 600 s each were obtained on February 27, 2020, the total exposure time was 50 min; on April 24, 2020, we obtained two spectral images with an exposure time of 1200 s each in VPHG600G and three spectral images with an exposure time of 1200 s each in VPHG600R, the total exposure time was 100 min.

Fourteen narrow hydrogen, oxygen, nitrogen, sulfur, and helium emission lines are seen in our spectrum (Fig. 5). Information on these lines is collected in Table 6. The redshift of the galaxy determined from these 14 lines is $z = 0.11425 \pm 0.00031$. The ratios $\log([\text{N II}]\lambda 6584/H\alpha) = -0.61 \pm 0.03$ and $\log([\text{O III}]\lambda 5007/H\beta) = 0.88 \pm 0.05$. From the position on the BPT diagram (Fig. 9) and the absence of broad lines, the object is classified as a Seyfert 2 galaxy.

An appreciable absorption is detected in the

SRGA J043209.6+354917

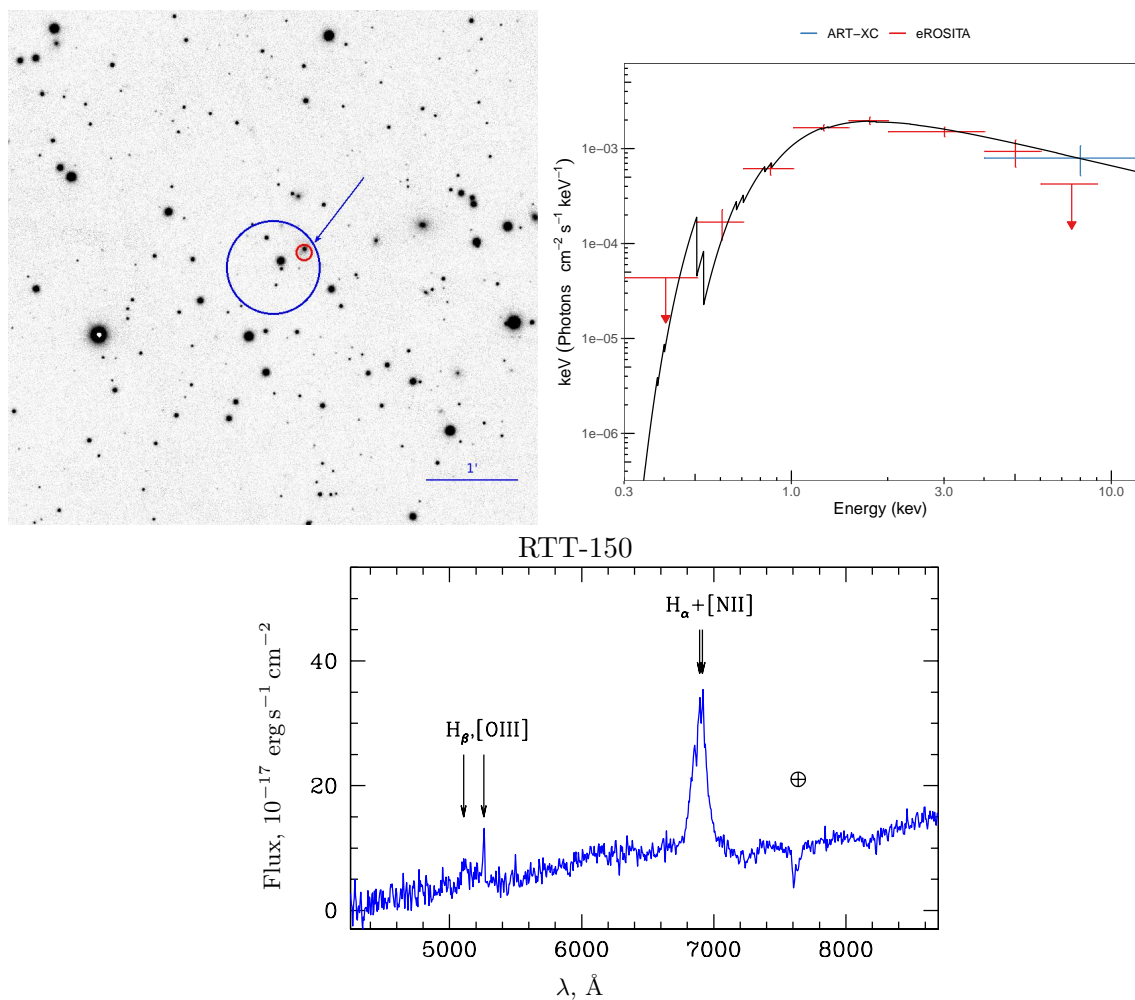


Fig. 3. Same as Fig. 1, but for SRGA J043209.6+354917. In the pointing picture the blue and red circumferences indicate the ART-XC and eROSITA position error circles, respectively.

Line	Wavelength, Å	Flux, 10^{-16} erg s $^{-1}$ cm $^{-2}$	Eq. Width, Å	$FWHM$, km s $^{-1}$
H β , narrow	5112	< 2	> -4.3	—
H β , broad	5112	28 ± 7	-64 ± 16	$(5.8 \pm 0.6) \times 10^3$
O III λ 4960	—	< 3	> -6.5	—
O III λ 5007	5260	12 ± 2	-27 ± 5	$(6.4 \pm 1.2) \times 10^2$
N II λ 6548	6854	2 ± 2	-2 ± 2	$(5.8 \pm 0.9) \times 10^2$
H α , narrow	6893	9 ± 2	-9 ± 2	$(5.8 \pm 0.9) \times 10^2$
H α , broad	6893	282 ± 8	-278 ± 8	$(6.0 \pm 0.2) \times 10^3$
N II λ 6584	6919	14 ± 2	-14 ± 2	$(5.8 \pm 0.9) \times 10^2$

Table 4. Spectral features of SRGA J043209.6+354917 = 2MASXJ04320796+3549287

SRGA J045049.8+301449

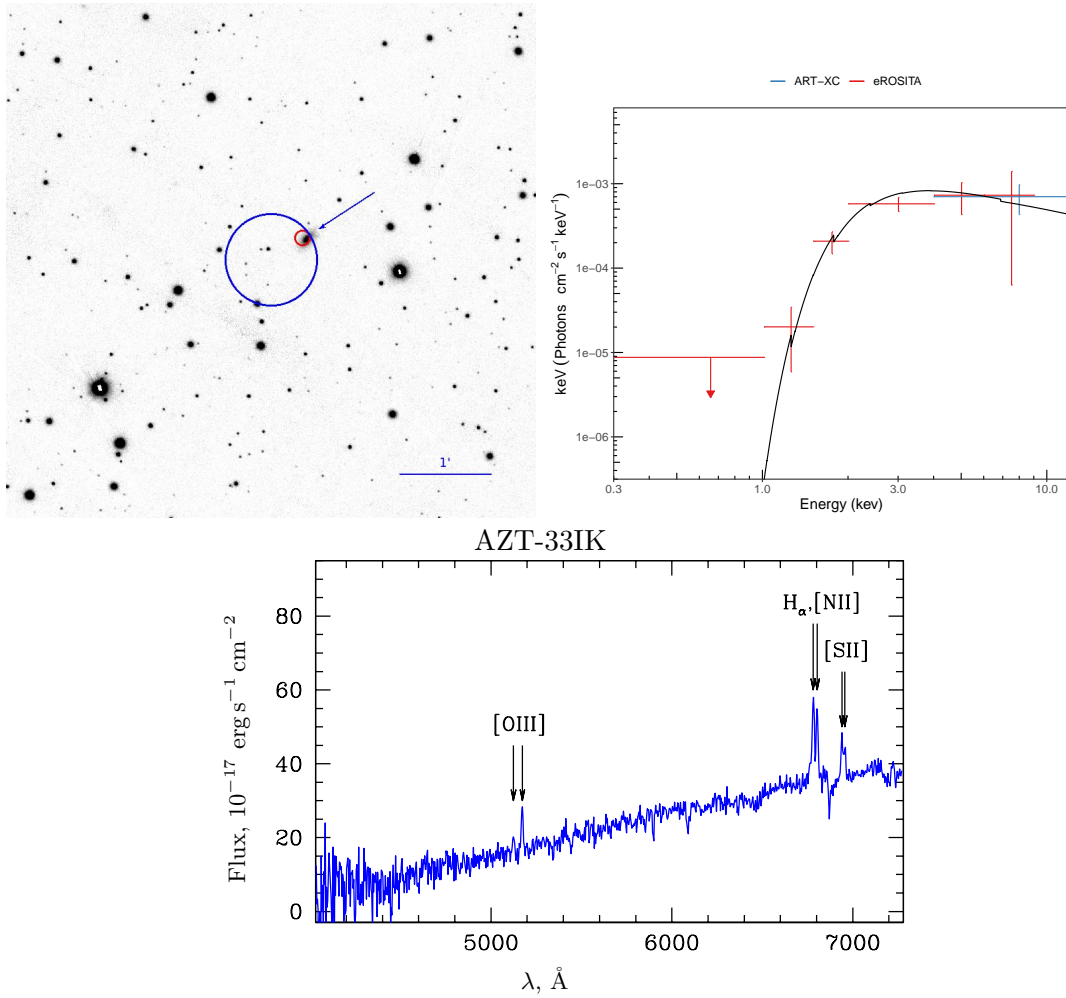


Fig. 4. Same as Fig. 3, but for SRGA J045049.8+301449.

Line	Wavelength, Å	Flux, $10^{-16} \text{ erg s}^{-1} \text{ cm}^{-2}$	Eq. Width, Å	$FWHM$, km s^{-1}
H β	5037	< 2	> -1.3	—
O III λ 4960	5124	5.9 ± 0.8	-3.7 ± 0.5	$(6.5 \pm 0.6) \times 10^2$
O III λ 5007	5173	17 ± 2	-10.3 ± 1.2	$(6.8 \pm 0.6) \times 10^2$
H α , narrow	6781	24 ± 8	-7 ± 2	$(4.7 \pm 0.5) \times 10^2$
H α , broad	6781	25 ± 4	-7.1 ± 1.2	$(2.8 \pm 0.4) \times 10^3$
N II λ 6584	6803	22 ± 3	-6.7 ± 0.9	$(4.8 \pm 0.5) \times 10^2$
S II λ 6718	6940	15 ± 2	-4.2 ± 0.6	$(5.2 \pm 0.8) \times 10^2$
S II λ 6732	6956	10 ± 2	-2.7 ± 0.6	$(4.8 \pm 0.8) \times 10^2$

Table 5. Spectral features of SRGA J045049.8+301449 = LEDA 1896296

SRGA J152102.3+320418

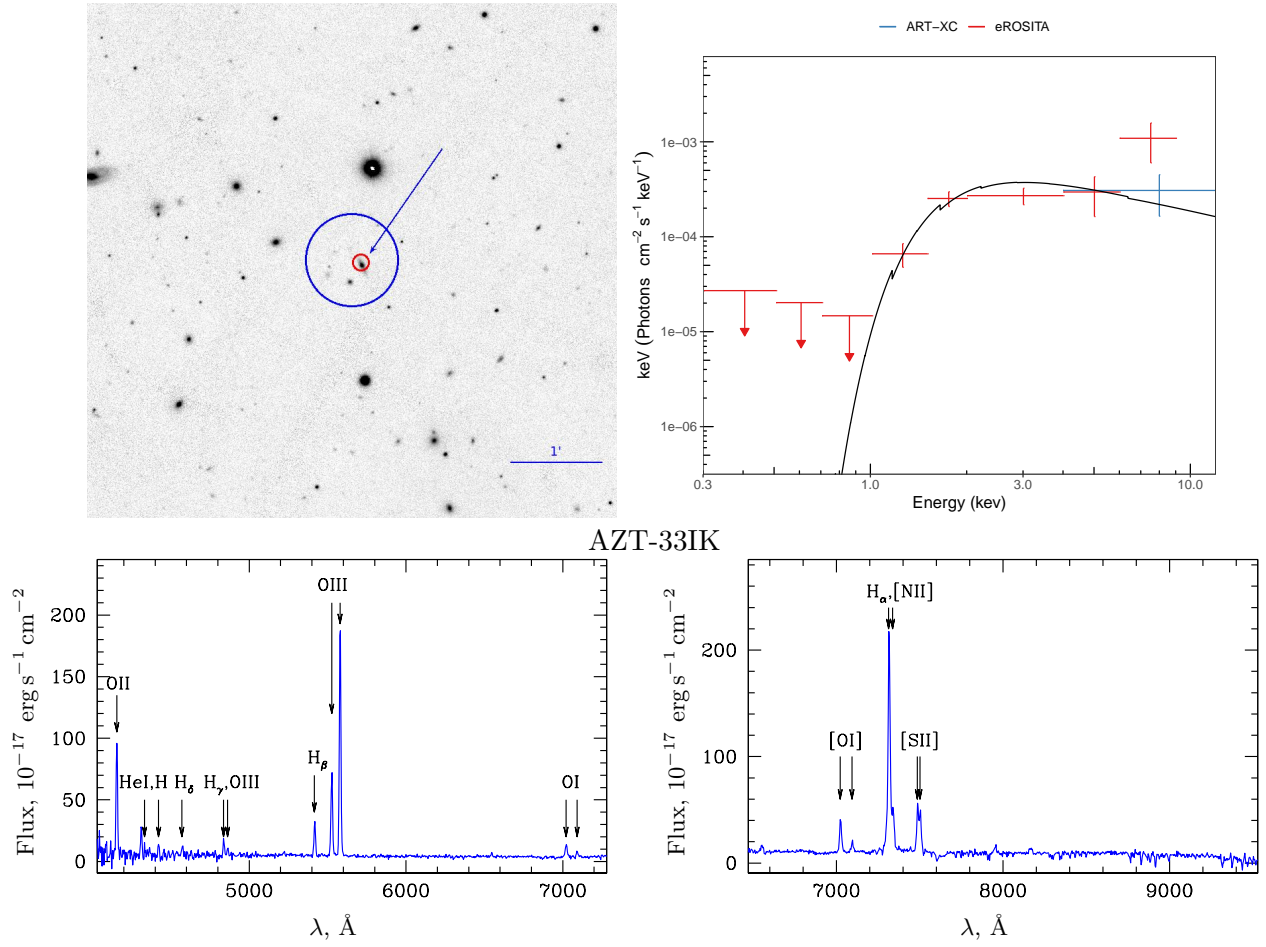


Fig. 5. Same as Fig. 3, but for SRGA J152102.3+320418. The optical spectrum is shown on the two lower panels: the spectrum taken in VPGH600G (left) and VPHG600R (right).

Line	Wavelength, Å	Flux, 10^{-16} erg s $^{-1}$ cm $^{-2}$	Eq. Width, Å	$FWHM$, km s $^{-1}$
OII λ 3729	4155	112 ± 7	$(-1.8^{+1.7}_{-0.8}) \times 10^2$	$(6.8 \pm 0.8) \times 10^2$
HeI λ 3889	4312	33 ± 7	-9^{+9}_{-4}	$(6.2 \pm 0.8) \times 10^2$
H δ	4573	< 11	> -27	—
H γ	4837	14 ± 2	-31^{+12}_{-6}	$(6.7 \pm 0.7) \times 10^2$
O III λ 4364	4863	7.1 ± 1.5	$-15.4^{+1.2}_{-2.7}$	$(6.3 \pm 0.7) \times 10^2$
H β	5418	30 ± 3	-67^{+24}_{-13}	$(5.7 \pm 0.6) \times 10^2$
O III λ 4960	5527	75 ± 3	$(-1.23^{+0.45}_{-0.11}) \times 10^2$	$(6.1 \pm 0.6) \times 10^2$
O III λ 5007	5580	$(2.3 \pm 0.1) \cdot 10^2$	$(-3.6 \pm 0.4) \times 10^2$	$(6.3 \pm 0.6) \times 10^2$
O I λ 6302	7022	14.9 ± 0.7	-41^{+8}_{-7}	$(6.1 \pm 0.5) \times 10^2$
O I λ 6365	7086	< 7	> -7.6	—
N II λ 6548	7298	< 20	> -22	—
H α	7316	$(3.0 \pm 0.1) \cdot 10^2$	$(-2.4^{+0.8}_{-0.7}) \times 10^2$	$(5.6 \pm 0.4) \times 10^2$
N II λ 6584	7339	73 ± 4	-56^{+29}_{-28}	$(7.2 \pm 0.8) \times 10^2$
S II λ 6718	7487	62 ± 7	-58 ± 8	$(5.9 \pm 0.4) \times 10^2$
S II λ 6732	7504	53 ± 7	-50 ± 8	$(5.8 \pm 0.4) \times 10^2$

Table 6. Spectral features of SRGA J152102.3+320418 = WISEA J152101.83+320414.6

object's X-ray spectrum (Fig. 5): $N_{\text{H}} \sim 2.5 \times 10^{22} \text{ cm}^{-2}$.

SRGA J200431.6+610211

This X-ray source was discovered during the ROSAT all-sky survey: 2RXS J200433.8+610235 (Boller et al., 2016). However, its nature so far has remained unknown. The source was detected by both ART-XC and eROSITA telescopes of the SRG observatory.

The X-ray source is reliably identified (Fig. 6) with the galaxy 2MASX J20043237+6102311 = WISEA J200432.40+610230.8, whose infrared color ($W1 - W2 = 0.89$) points to the possible presence of an active nucleus.

Our optical observations were carried out on October 22, 2020, at the AZT-33IK telescope using VPHG600G. Five spectral images with an exposure time of 300 s each were obtained; the total exposure time was 25 min.

Narrow $\text{H}\beta$, $[\text{O III}]\lambda 4959$, $[\text{O III}]\lambda 5007$, $\text{H}\alpha$, $[\text{N II}]\lambda 6584$, and sulfur doublet emission lines are seen in our spectrum (Fig. 6). The line characteristics are given in Table 7. The redshift was determined from seven lines: $z = 0.05866 \pm 0.00013$.

The ratios $\log([\text{O III}]\lambda 5007/\text{H}\beta) = 1.04 \pm 0.03$ and $\log([\text{N II}]\lambda 6584/\text{H}\alpha) = 0.00 \pm 0.06$. From the position on the BPT diagram (Fig. 9) and the absence of broad lines, the object can be classified as a Seyfert 2 galaxy.

A slight absorption is detected in the object's X-ray spectrum (Fig. 6): $N_{\text{H}} \sim 5 \times 10^{21} \text{ cm}^{-2}$.

SRGA J224125.9+760343

This X-ray source was discovered during the ROSAT all-sky survey: 2RXS J224124.5+760346 (Boller et al., 2016), but its nature so far has remained unknown. The source was detected by both ART-XC and eROSITA telescopes of the SRG observatory.

The X-ray source is reliably identified (Fig. 7) with the infrared source WISEA J224125.79+760353.8, whose infrared color ($W1 - W2 = 0.97$) points to the possible presence of an active nucleus.

Our optical observations were carried out on June 21, 2020, at RTT-150. Three spectral images with an exposure time of 1800 s each were obtained; the total exposure time was 90 min.

The Balmer $\text{H}\alpha$, $\text{H}\beta$, $\text{H}\gamma$, and $\text{H}\delta$, emission lines with narrow and broad components are seen in our spectrum (Fig. 7). The $\text{H}\alpha$ line merged with the $[\text{N II}]\lambda 6548$ and $[\text{N II}]\lambda 6584$ lines. Obviously, for this reason, the measured $FWHM$ of the broad $\text{H}\alpha$ component slightly exceeds the $FWHM$ of the

corresponding $\text{H}\beta$ component. The $[\text{O III}]\lambda 4960$, $[\text{O III}]\lambda 5007$ emission lines and the complex of $\text{Fe II}\lambda 4570$ ($\lambda 4434$ – $\lambda 4684$) lines are also present in the spectrum. The characteristics of all lines are presented in Table 8. The redshift determined from six emission lines is $z = 0.2834 \pm 0.0003$. The narrow-line flux ratio is $\log([\text{O III}]\lambda 5007/\text{H}\beta) = 0.66$, while the ratio $\log([\text{N II}]\lambda 6584/\text{H}\alpha)$ is difficult to estimate due to the line merging. The relative narrowness of the broad Balmer line components ($FWHM(\text{H}\beta) < 2000 \text{ km s}^{-1}$) and the presence of a noticeable Fe II emission suggest that this object is a narrow-line Seyfert 1 galaxy.

There is no evidence of an additional absorption in the object's X-ray spectrum (Fig. 7), except for the absorption in our Galaxy. At a fixed slope of the power-law spectrum $\Gamma = 1.8$ we obtain a strict upper limit on the internal absorption: $N_{\text{H}} < 4 \times 10^{20} \text{ cm}^{-2}$.

SRGA J232446.8+440756

This X-ray source was discovered in the 4–12 keV band by the ART-XC telescope of the SRG observatory and, at the same time, was not detected in softer X-rays by the eROSITA telescope.

The X-ray source can be identified with the irregular galaxy 2MASX J23244834+4407564 = WISEA J232448.36+440756.5 (Fig. 8). Its redshift is known: $z = 0.04634$ (Huchra et al., 2012), while its infrared color ($W1 - W2 = 0.83$) points to the presence of an active nucleus. However, the galaxy has not yet been classified as an AGN from optical spectroscopy.

Our optical observations were carried out on June 10, 2020, at RTT-150. Nine spectral images with an exposure of 600 s each were obtained; the total exposure time was 90 min.

Narrow $\text{H}\alpha$, $\text{H}\beta$, $[\text{O III}]\lambda 4959$, $\lambda 5007$, $[\text{N II}]\lambda 6584$ emission lines and the $[\text{S II}]$ doublet are seen in our spectrum (Fig. 8). The line characteristics are given in Table 9. The redshift was determined from five emission lines and is $z = 0.04624 \pm 0.00020$, consistent with the previously measured value by Huchra et al. (2012). The ratios $\log([\text{N II}]\lambda 6584/\text{H}\alpha) = -0.46 \pm 0.07$ and $\log([\text{O III}]\lambda 5007/\text{H}\beta) = 0.86 \pm 0.07$. From the position on the BPT diagram (Fig. 9) and the absence of broad lines, the object can be classified as a Seyfert 2 galaxy.

The non-detection by the eROSITA telescope in combination with the 4–12 keV flux measured by the ART-XC telescope (Fig. 8) allows a strict upper limit to be placed on the absorption column density: $N_{\text{H}} > 3 \times 10^{23} \text{ cm}^{-2}$.

SRGA J200431.6+610211

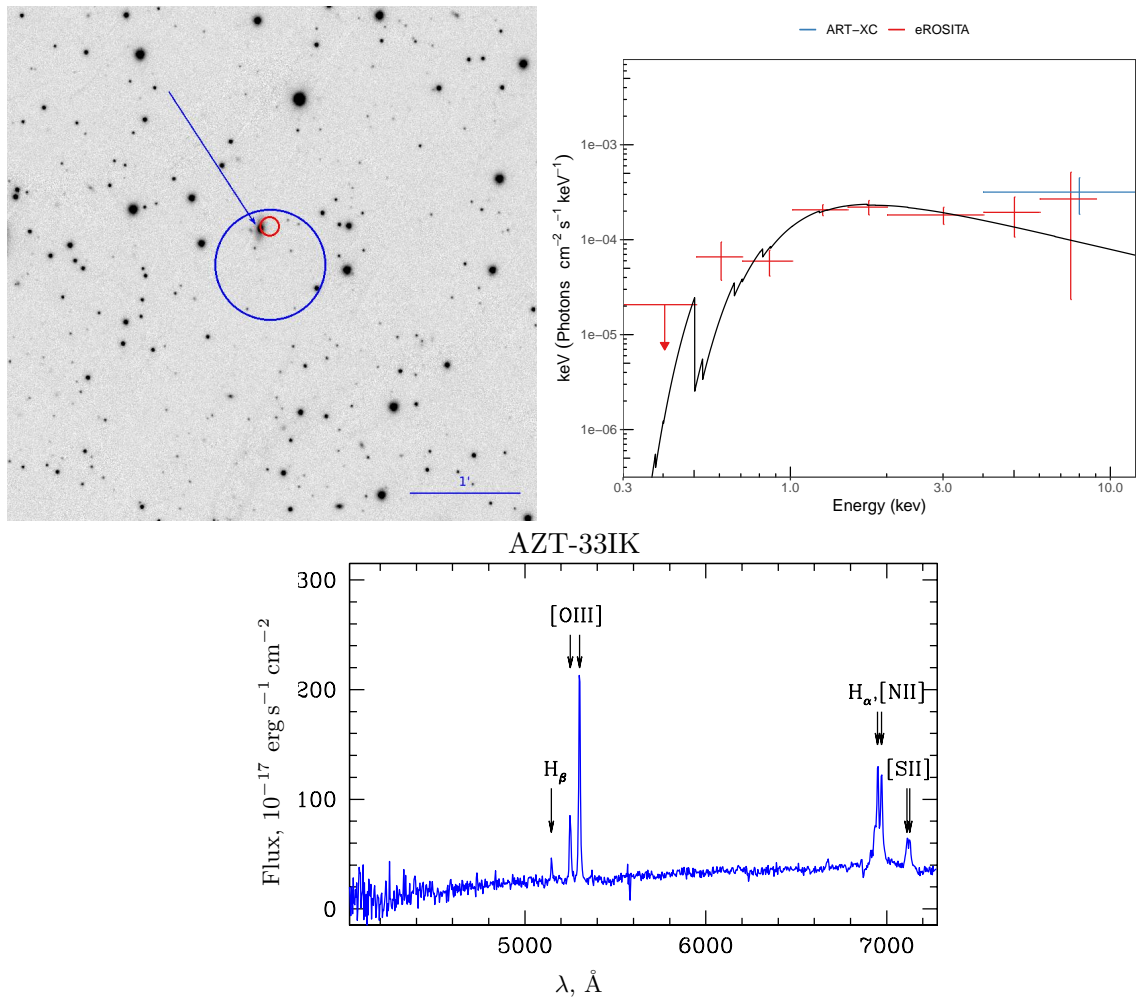


Fig. 6. Same as Fig. 3, but for SRGA J200431.6 + 610211.

Line	Wavelength, Å	Flux, $10^{-16} \text{ erg s}^{-1} \text{ cm}^{-2}$	Eq. Width, Å	$FWHM$, km s^{-1}
H β	5147	18.0 ± 1.2	-6.7 ± 0.5	$(4.7 \pm 0.7) \times 10^2$
O III λ 4959	5250	57 ± 5	-19 ± 4	$(4.8 \pm 0.7) \times 10^2$
O III λ 5007	5302	196 ± 7	-59 ± 3	$(4.8 \pm 0.7) \times 10^2$
H α	6950	110 ± 11	-23 ± 2	$(4.7 \pm 0.5) \times 10^2$
N II λ 6584	6972	111 ± 11	-23 ± 2	$(5.0 \pm 0.5) \times 10^2$
S II λ 6718	7113	31 ± 3	-7.7 ± 0.6	$(5.5 \pm 0.4) \times 10^2$
S II λ 6732	7129	31 ± 3	-7.7 ± 0.6	$(5.2 \pm 0.4) \times 10^2$

Table 7. Spectral features of SRGA J200431.6+610211 = 2MASX J20043237+6102311

SRGA J224125.9+760343

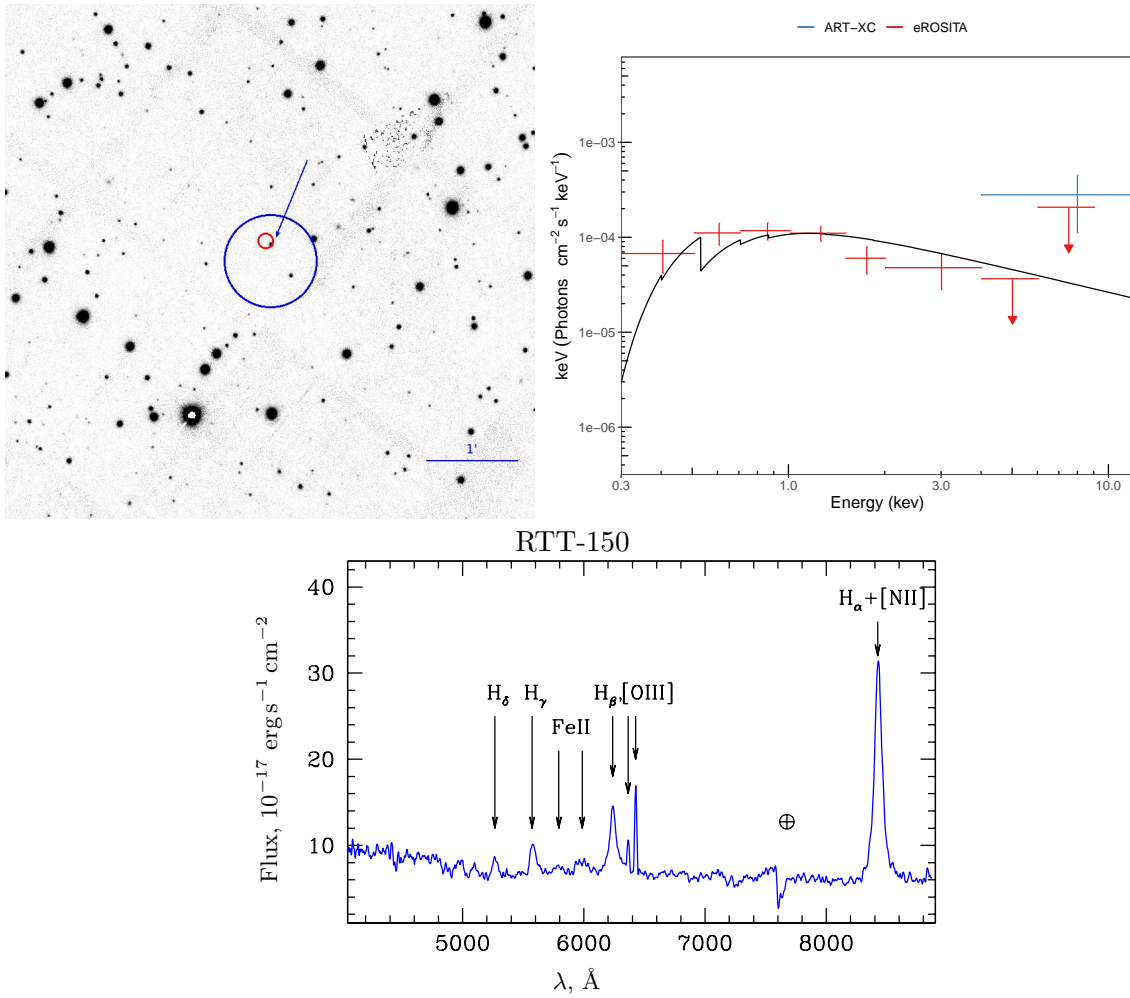


Fig. 7. Same as Fig. 3, but for SRGA J224125.9+760343. In contrast to other sources, we show the power-law model with a slope $\Gamma = 2.4$ that provides a better quality of the fit than does the model with the standard slope $\Gamma = 1.8$.

Line	Wavelength, Å	Flux, $10^{-16} \text{ erg s}^{-1} \text{ cm}^{-2}$	Eq. Width	$FWHM$, km s^{-1}
H γ , narrow	5579	< 0.8	> -1.2	—
H γ , broad	5579	17.4 ± 0.8	-26 ± 1	$(2.1 \pm 0.2) \times 10^3$
FeII λ 4570	5982	18.6 ± 1.3	—	—
H β , narrow	6239	4.4 ± 0.3	-6.4 ± 0.4	$(3.8 \pm 0.9) \times 10^2$
H β , broad	6239	51 ± 1	-35 ± 2	$(1.5 \pm 0.2) \times 10^3$
O III λ 4959	6365	7.7 ± 0.2	-11.3 ± 0.3	$(3.7 \pm 0.9) \times 10^2$
O III λ 5007	6428	20.1 ± 0.3	-29 ± 1	$(3.7 \pm 0.9) \times 10^2$
H α , narrow	8429	6.0 ± 0.9	-8.8 ± 1.3	$(2.8 \pm 0.7) \times 10^2$
H α , broad	8429	197 ± 3	-288 ± 5	$(2.3 \pm 0.1) \times 10^3$

Table 8. Spectral features of SRGA J224125.9+760343 = WISEA J224125.79+760353.8

SRGA J232446.8+440756

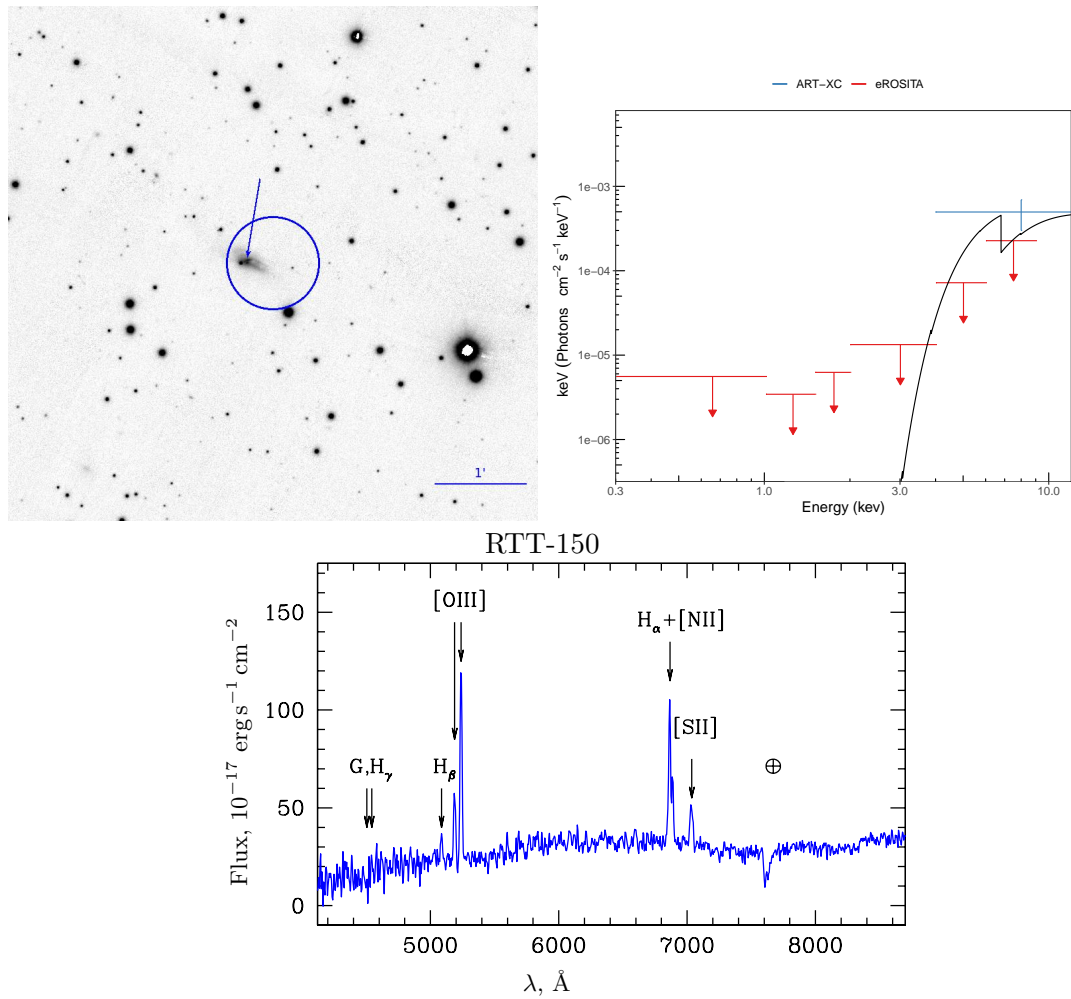


Fig. 8. Same as Fig. 1, but for SRGA J232446.8+440756.

Line	Wavelength, Å	Flux, $10^{-16} \text{ erg s}^{-1} \text{ cm}^{-2}$	Eq. Width, Å	$FWHM$, km s^{-1}
H β	5087	27 ± 4	-12 ± 3	$(7.4 \pm 1.0) \times 10^2$
O III λ 4959	5189	74 ± 9	-42 ± 9	$(6.8 \pm 1.0) \times 10^2$
O III λ 5007	5239	196 ± 12	-102 ± 17	$(7.3 \pm 1.0) \times 10^2$
H α	6865	134 ± 9	-41 ± 6	$(5.3 \pm 0.8) \times 10^2$
N II λ 6584	6887	46 ± 7	-17 ± 3	$(1.5^{+3.7}_{-1.5}) \times 10^2$

Table 9. Spectral features of SRGA J232446.8+440756 = 2MASX J23244834+4407564

PROPERTIES OF THE DETECTED AGNS

Table 10 presents the main properties of the AGNs that we managed to identify in this study. Apart from the redshift and the optical type, the estimated column density of cold matter inside the object NH and its X-ray luminosity L_X in the 4–12 keV energy band are given for each object.

We estimated the X-ray luminosity based on the flux in the 4–12 keV energy band measured by the ART-XC telescope of the SRG observatory and the photometric distance to the object calculated from its redshift. The presented values of L_X neglect the k-corrections and were not corrected for the line of sight absorption. The first of these corrections should not be significant, given the low redshifts of the objects and that the slope of the AGN X-ray spectra does not differ greatly from $\Gamma = 2$. As regards the absorption correction, although it may turn out to be large for three objects from the sample with a high column density ($N_H > 10^{23} \text{ cm}^{-2}$), it is virtually impossible to reliably take into account based on the existing ART-XC and eROSITA data (there are too few detected photons). Therefore, it should be kept in mind that the true luminosity of these heavily obscured AGNs can be greater than that given in the table by several times.

As can be seen from Table 10, most of the objects being discussed are Seyfert galaxies with a luminosity $L_X \sim 10^{42}–10^{44} \text{ erg s}^{-1}$ in the nearby Universe ($z < 0.1$), except for the source SRGA J224125.9+760343 at $z = 0.28$ with a luminosity $L_X \sim 10^{45} \text{ erg s}^{-1}$ that, using the traditional terminology, may be attributed to quasars.

Almost all of the investigated objects fall into the region of Seyfert galaxies on the standard BPT diagram (Fig. 9) of the [O III] $\lambda 5007/\text{H}\beta$ and [N II] $\lambda 6584/\text{H}\alpha$ flux ratios. SRGAJ005751.0+210846 was not placed on this diagram, because the required information about the emission lines cannot be obtained from the available optical spectra. In this case, we are dealing with a galaxy (LEDA 1643776) seen edge-on, so that the line emission regions in its active nucleus can be completely hidden from the observer. SRGAJ224125.9+760343 did not fall on the BPT diagram either, because the broad $\text{H}\alpha$ component merged with the [N II] $\lambda 6584$ line and, for this reason, it is impossible to estimate the line parameters. Undoubtedly, both objects are AGNs, because they are characterized by a high X-ray luminosity. As has already been discussed above, the object SRGAJ014157.0–032915 is located on the BPT diagram in the region of star-forming galaxies, but near the region of Seyfert

galaxies. The narrow emission lines in its spectrum probably result not only from the accretion of matter onto the SMBH in the galactic nucleus, but also from intense star formation in the galaxy.

Six of the eight investigated object(if SRGA J005751.0 + 210846 seen edge-on is included) turned out to be Seyfert 2 or intermediate type (1.9) galaxies. The detection of an appreciable absorption in their X-ray spectra is quite expectable.

One of the objects (SRGA J224125.9+760343) turned out to be a narrow-line Seyfert 2 galaxy. We can estimate the SMBH mass in this object from the formula (Vestergaard and Peterson, 2006)

$$\lg M_{\text{BH}} = \lg \left[\left(\frac{FWHM(\text{H}\beta)}{1000 \text{ km/s}} \right)^2 \left(\frac{L(\text{H}\beta)}{10^{42} \text{ erg/s}} \right)^{0.63} \right] + 6.67.$$

In our case, $FWHM(\text{H}\beta) = (1.5 \pm 0.2) \times 10^3 \text{ km s}^{-1}$ and the line flux is $F(\text{H}\beta) = (1.30 \pm 0.02) \times 10^{-14} \text{ erg s}^{-1} \text{ cm}^{-2}$ (see Table. 8), which allows the line luminosity to be estimated at $z = 0.2834$, $L(\text{H}\beta) \approx 3.3 \times 10^{42} \text{ erg s}^{-1}$. As a result, we find $M_{\text{BH}} \approx 2.3 \times 10^7 M_\odot$.

For such a relatively small black hole the critical Eddington luminosity is $L_{\text{Edd}} \approx 3 \times 10^{45} \text{ erg s}^{-1}$. At the same time, the measured luminosity of the source SRGAJ224125.9+760343 in the X-ray energy band (4–12 keV) is $L_X \sim (2 - 13) \cdot 10^{44} \text{ erg s}^{-1}$. Since the bolometric luminosity L_{bol} of an AGN usually exceeds the X-ray luminosity at least by several times (see, e.g., Sazonov et al., 2004), we conclude that $L_{\text{bol}} \sim L_{\text{Edd}}$ for SRGA J224125.9+760343. This corresponds to the universally accepted paradigm (see, e.g., Mathur, 2000) that in narrow-line Seyfert 1 galaxies the accretion of matter occurs at a rate close to the critical one.

CONCLUSIONS

We have identified eight new AGNs among the X-ray sources detected during the first all-sky survey with the ART-XC telescope aboard the SRG observatory. We measured the redshifts of these objects and studied their optical and X-ray properties. Most of the objects turned out to be Seyfert 2 galaxies and exhibit significant absorption in the X-ray spectrum. For three AGNs, the absorption column density exceeds $3 \times 10^{23} \text{ cm}^{-2}$. For this reason, they are detected only in fairly hard X-rays with the ART-XC telescope and are not detected in softer X-rays with eROSITA. In one of these

Object	Optical type ¹	z	N_{H}^2	$\log L_{\mathrm{X}}^3$
SRGA J005751.0+210846	Sy2 ⁴	0.04798 ± 0.00002	$> 1 \times 10^3$	$43.7^{+0.2}_{-0.3}$
SRGA J014157.0-032915	Sy2	0.01878 ± 0.00003	$> 3 \times 10^2$	$42.5^{+0.3}_{-1.2}$
SRGA J043209.6+354917	Sy1	0.0506 ± 0.0010	$3.0^{+0.8}_{-0.7}$	$43.8^{+0.2}_{-0.3}$
SRGA J045049.8+301449	Sy1.9	0.03308 ± 0.00004	38^{+11}_{-10}	$43.4^{+0.2}_{-0.3}$
SRGA J152102.3+320418	Sy2	0.1143 ± 0.0003	25^{+6}_{-6}	$44.1^{+0.2}_{-0.4}$
SRGA J200431.6+610211	Sy2	0.05866 ± 0.00013	$4.7^{+2.2}_{-1.4}$	$43.6^{+0.2}_{-0.3}$
SRGA J224125.9+760343	NLSy1	0.2834 ± 0.0004	< 0.4	$44.9^{+0.2}_{-0.6}$
SRGA J232446.8+440756	Sy2	0.0462 ± 0.0002	$> 3 \times 10^2$	$43.5^{+0.2}_{-0.3}$

¹ Sy1, Sy1.9, and Sy2 are Seyfert 1, 1.9, and 2 galaxies, respectively, NLSy1 is a narrow-line Seyfert 1 galaxy.

² In units of 10^{21} cm^{-2} , the errors and limits correspond to the 90% confidence level, while the 68% confidence level is presented for the source SRGA J014157.0-032915.

³ The luminosity uncorrected for absorption in the observed 4–12 keV energy band in units of erg s^{-1} .

⁴ The classification is arbitrary, because the galaxy is seen edge-on.

Table 10. Properties of the AGNs

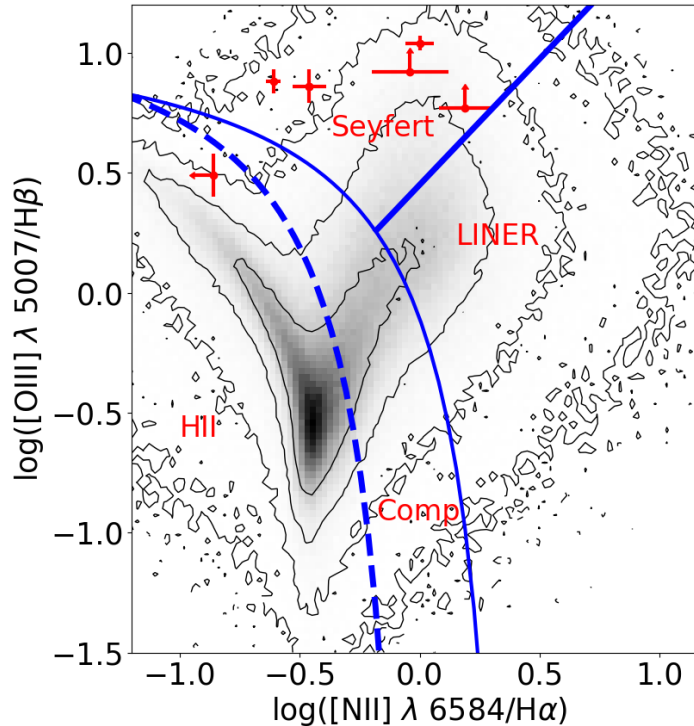


Fig. 9. Positions of the AGNs under study (red dots and limits) on the BPT diagram (Baldwin et al., 1981) constructed from SDSS data (release 7, SDSS Collaboration 2009). The demarcation lines between different classes of galaxies were taken from Kauffmann et al. (2003) – the dashed line, Kewley et al. (2001) – the thin line, and Schawinski et al. (2007) – the thick line. Only the six objects for which we managed to determine the parameters of the required lines are shown. The diagram was constructed with the help of the site http://wwwmpa.mpa-garching.mpg.de/SDSS/DR7/Data/gal_line_dr7_v5_2.fit.gz.

objects (SRGA J005751.0+210846) the absorption may be associated mainly with the interstellar gas in the host galaxy seen edge-on. One of the objects (SRGA J224125.9+760343) turned out to be a narrow-line Seyfert 1 galaxy with a luminosity close to the Eddington limit.

The results of this study confirm the expectations that the ART-XC telescope is an efficient instrument for searches of heavily obscured and other interesting AGNs in the relatively nearby ($z \lesssim 0.3$) Universe. The SRG all-sky survey will last for more than three years more, which will allow a lot of such objects to be discovered.

ACKNOWLEDGMENTS

This work was supported by RSF grant no. 19-12-00396. We thank TÜBİTAK, the Space Research Institute of the Russian Academy of Sciences, the Kazan Federal University, and the Academy of Sciences of Tatarstan for supporting the observations at the Russian–Turkish 1.5-m telescope (RTT-150). The measurements with the AZT-33IK telescope were performed within the basic financing of the FNI II.16 program and were obtained using the equipment of the Angara sharing center⁶. The work of I.F. Bikmaev, E.N. Irtuganov, and E.A. Nikolaeva was supported by the subsidy (project no. 0671-2020-0052) allocated to the Kazan Federal University for a State assignment in the sphere of scientific activities. In this study we used observational data from the eROSITA telescope onboard the SRG observatory. The SRG observatory was built by Roskosmos in the interests of the Russian Academy of Sciences represented by its Space Research Institute (IKI) within the framework of the Russian Federal Space Program, with the participation of the Deutsches Zentrum für Luft- und Raumfahrt (DLR). The SRG/eROSITA X-ray telescope was built by a consortium of German Institutes led by MPE, and supported by DLR. The SRG spacecraft was designed, built, launched, and is operated by the Lavochkin Association and its subcontractors. The science data are downlinked via the Deep Space Network Antennae in Bear Lakes, Ussurijsk, and Baykonur, funded by Roskosmos. The eROSITA data used in this work were processed using the eSASS software system developed by the German eROSITA consortium and the proprietary data reduction and analysis software developed by the Russian eROSITA Consortium.

⁶<http://ckp-rf.ru/ckp/3056/>

REFERENCES

1. V.L. Afanasiev, S.N. Dodonov, V.R. Amirkhanyan, A.V. Moiseev, *Astrophys. Bull.* 71, 514 (2016).
2. J.A. Baldwin, M.M. Phillips, R. Terlevich, *Publ. Astron. Soc. Pacific* 93, (1981).
3. N. Ben Bekhti, L. Flöer, R. Keller, J. Kerp, D. Lenz, B. Winkel, et al., *Astron. Astrophys.* 594, A116 (2016).
4. Th. Boller, M.J. Freyberg, J. Trümper, F. Haberl, W. Voges, and K. Nandra, *Astron. Astrophys.* 588, A103 (2016).
5. R.A. Burenin, A.L. Amvrosov, M.V. Eiselevich, V.M. Grigor'ev, V.A. Aref'ev, V.S. Vorob'ev, et al., *Astron. Letters* 42, 5 (2016).
6. K.C. Chambers, E.A. Magnier, N. Metcalfe, H.A. Flewelling, M.E. Huber, C.Z. Waters, et al., [arxiv.org:1612.05560.pdf](https://arxiv.org/abs/1612.05560). (2016).
7. P.A. Evans, K.L. Page, J.P. Osborne, A.P. Beardmore, R. Willingale, D.N. Burrows, et al., *Astrophys. J. Suppl. Ser.* 247, 2 (2020).
8. J.P. Huchra, L.M. Macri, K.L. Masters, T.H. Jarrett, P.C. Berlind, M. Calkins, A.C. Crook, et al., *Astrophys. J. Suppl. Ser.* 199, 2 (2012).
9. G. Kauffmann, T.M. Heckman, C. Tremonti, J. Brinchmann, S. Charlot, S.D.M. White, et al., *MNRAS*. 346, 4 (2003).
10. L.J. Kewley, M.A. Dopita, R.S. Sutherland, C.A. Heisler, and J. Trevena, *Astron. J.* 556, 1 (2001).
11. S. Mathur, *MNRAS*. 314, 4 (2000).
12. K. Oh, M. Koss, C.B. Kwardt, K. Schawinski, W.H. Baumgartner, S.D. Barthelmy et al., *Astrophys. J. Suppl. Ser.* 235, 1 (2018).
13. D.E. Osterbrock, *Astrophys. J.* 241, 462 (1981).
14. M. Pavlinsky, A. Tkachenko, V. Levin, N. Alexandrovich, V. Arefiev, V. Babyshkin, et al., *Astron. Astrophys.* in press, (2021); [arxiv.org:2103.12479.pdf](https://arxiv.org/abs/2103.12479).
15. P. Predehl, R. Andritschke, V. Arefiev, V. Babyshkin, O. Batanov, M. Becker, et al., *Astron. Astrophys.* in press, (2020); [arxiv.org:2010.03477.pdf](https://arxiv.org/abs/2010.03477).
16. S.Yu. Sazonov, J.P. Ostriker, and R.A. Sunyaev, *MNRAS*. 347, 1 (2004).
17. K. Schawinski, D. Thomas, M. Sarzi, C. Maraston, S. Kaviraj, S.-J. Joo, S.K. Yi, and J. Silk, *MNRAS*. 382, 4 (2007).
18. SDSS Collaboration, *Astrophys. J. Suppl. Ser.* 182, 2 (2009). [SDSS Collaboration: K.N. Abazajian, J.K. Adelman-McCarthy, M.A. Agüeros, S.S. Allam, P.C. Allende Prieto et al.]
19. SDSS Collaboration: S. Alam, F.D. Albareti, P.C. Allende, F. Anders, S.F. Anderson, et al., *Astrophys. J. Suppl. Ser.* 219, 1 (2015).
20. SDSS Collaboration: F.D. Albareti, C.A. Prieto, A. Almeida, et al., *Astrophys. J. Suppl. Ser.* 233, 25 (2017). [SDSS Collaboration: F.D. Albareti, C.A. Prieto, A. Almeida, et al.]

21. R.A. Sunyaev et al., 2021, in press , (2021).
22. M.-P. Véron-Cetty, P. Véron, and A.C. Gonçalves, *Astron. Astrophys.* 372, (2001).
23. M. Vestergaard and B.M. Peterson, *Astron. Astrophys.* 641, 2 (2006).
24. N.E. White, P. Giommi, and L. Angelini, *VizieR On-line Data Catalog IX/31*, (2000).
25. E.L. Wright, P.R.M. Eisenhardt, A.K. Mainzer, M.E. Ressler, R.M. Cutri, T. Jarrett, J.D. Kirkpatrick, D. Padgett, et al., *Astron. J.* 140, 1868 (2010).
26. The XMM-Newton Survey Science Centre, *VizieR On-line Data Catalog IX/53*, (2018).